Wireless operational modal analysis of a multi-span prestressed concrete bridge for structural identification

Matthew J. Whelan[1], Michael V. Gangone[1], Kerop D. Janoyan[2]*, Neil A. Hoult[3], Campbell R. Middleton[4] and Kenichi Soga[5]

[1]*Clarkson University, Potsdam, NY 13699, USA*
[2]*Department of Civil and Environmental Engineering, Clarkson University, Potsdam, NY 13699, USA*
[3]*Department of Civil Engineering, Queens University, Ontario K7L 3N6, Canada*
[4]*Structural Engineering with the Department of Engineering, University of Cambridge, CB2 1PZ, UK*
[5]*Civil Engineering with the Department of Engineering, University of Cambridge, CB2 1PZ, UK*

(Received October 14, 2009, Accepted January 18, 2010)

Abstract. Low-power radio frequency (RF) chip transceiver technology and the associated structural health monitoring platforms have matured recently to enable high-rate, lossless transmission of measurement data across large-scale sensor networks. The intrinsic value of these advanced capabilities is the allowance for high-quality, rapid operational modal analysis of in-service structures using distributed accelerometers to experimentally characterize the dynamic response. From the analysis afforded through these dynamic data sets, structural identification techniques can then be utilized to develop a well calibrated finite element (FE) model of the structure for baseline development, extended analytical structural evaluation, and load response assessment. This paper presents a case study in which operational modal analysis is performed on a three-span prestressed reinforced concrete bridge using a wireless sensor network. The low-power wireless platform deployed supported a high-rate, lossless transmission protocol enabling real-time remote acquisition of the vibration response as recorded by twenty-nine accelerometers at a 256 Sps sampling rate. Several instrumentation layouts were utilized to assess the global multi-span response using a stationary sensor array as well as the spatially refined response of a single span using roving sensors and reference-based techniques. Subsequent structural identification using FE modeling and iterative updating through comparison with the experimental analysis is then documented to demonstrate the inherent value in dynamic response measurement across structural systems using high-rate wireless sensor networks.

Keywords: structural health monitoring; ambient vibration testing; structural identification; bridge dynamics; wireless sensor networks.

1. Introduction

Analytical models of civil constructions are heavily utilized throughout the design and construction stages to safely predict allowable load capacities and service deflections. Furthermore, these computer-based mathematical representations are being extended to structural assessment, retrofit evaluation, and damage detection strategies as rehabilitation and life-cycle management have increasingly been pushed to the forefront of concern in civil engineering. While the governing

*Corresponding Author, Associate Professor, E-mail: kerop@clarkson.edu

dynamics of mechanical systems are well known and increasingly well predicted through advanced computing resources, the structural dynamics of large civil constructions, such as highway bridges, are complex and often poorly reconstructed with analytical models due to uncertainties in boundary conditions and idealization of mechanical aspects. The use of in-service experimental measurements to calibrate an analytical model based on indicators of the actual response can significantly improve the accuracy and validity of the conclusions derived from analysis of such models.

One of the fundamental benefits of ambient vibration testing of highway bridges is the ability to validate or dynamically calibrate analytical models of structural systems to optimize correlation with the measured response to develop a model that is more representative of the actual in-place, as-built condition. This process is known as structural identification and generally consists of developing a preliminary finite element model with reasonable detailing of the primary structural elements and then iteratively modifying model parameters to optimally minimize the difference between the predicted and measured modal parameters of a set of modes (Aktan *et al*. 1998, Morassi and Tonon 2008).

Acquiring the dynamic response measurements required for structural identification has been expedited through the development of low-power radio frequency (RF) instrumentation systems. High-rate wireless sensor networks (WSN) incorporating accelerometers offer the advantage of replacing costly, unwieldy cable-based systems to permit rapid in-service dynamic assessment of large structures and bridges. Small-form embedded systems with RF communication capabilities produce easily manageable instrumentation that can be quickly placed and repositioned to perform high-density reference-based operational modal analysis (OMA) in a very short time window. Until recently, data rate limitations and packet loss resulting from inefficient network transmission protocols limited the applicability of WSN for ambient vibration monitoring of structures. However, these early deficiencies have been overcome through leveraging advanced computing peripherals and efficient, robust network transmission protocols to achieve the high data rates and lossless reception required for OMA (Whelan and Janoyan 2009).

2. Experimental test details

2.1 Nine Wells Rail Bridge

The Nine Wells Rail Bridge on Addenbrooke's Access Road is a newly constructed bridge carrying the access road to Addenbrooke's Hospital in Cambridge, United Kingdom over an existing railway. The bridge consists of two travel lanes for traffic as well as a 4.2 m wide foot/cycle way along the entire length of the northernmost edge. There are three spans west-to-east of lengths 27.2 m, 28.3 m and 32.2 m referenced from centerline-to-centerline of the bearings (Fig. 1). Geometrically, the two westernmost spans are on a 1:20 slope, while the easternmost span is horizontal; all spans have a nominal nine degree skew. Each span consists of twelve precast 1700 mm deep prestressed concrete beams which support a 250 mm insitu reinforced concrete slab with an additional 125 mm layer of asphalt surfacing. The precast beams contain 27 standard prestressing strands of 15.2 mm diameter with a characteristic breaking load of 232 kN that were pretensioned to 70%, or 162.4 kN. All beams are supported by laminated rubber elastomeric bearings at the abutments and bedding mortar at the piers. A 1550 mm high by 400 mm wide precast reinforced concrete parapet lines each edge of the entire length of the bridge.

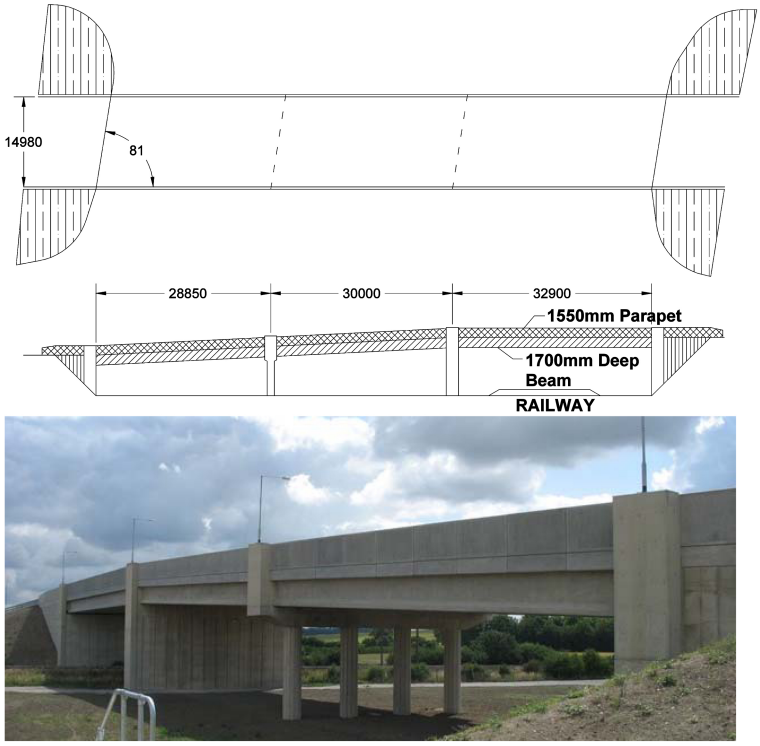

Fig. 1 Nine Wells Rail Bridge

2.2 Instrumentation and test details

A wireless sensor network was utilized to rapidly instrument the structure and remotely acquire high-rate, lossless data in real-time. The wireless sensing platform was developed by the authors at Clarkson University; the design and proprietary network protocol has been previously documented (Whelan and Janoyan 2009) and the system has been deployed on three field bridges in previous ambient vibration studies (Whelan *et al.* 2009a, 2009b). Wireless communication is facilitated by a proprietary network protocol implemented on a low-power RF chip transceiver employing direct sequence spread spectrum modulation over a 2.4 GHz carrier frequency. In this study, twenty channels sampled at a rate of 256 Sps per channel are supported within a single-hop, star topology network with further channel count expansion to the thirty total channels afforded through frequency division multiple access using an interrupt synchronized concurrent network.

2.2.1 Sensors and signal conditioning

ST Microelectronics LIS2L02AL low-noise capacitance-based accelerometers were distributed across the deck surface to record the ambient vibration response due to traffic loading. While this integrated circuit sensor is a dual-axis design, only the vertical acceleration was recorded to achieve the higher real-time sampling rates maintained over the low-power wireless network. The accelerometer has a ±2 g full-scale range, 30 μg/√Hz noise density, and nominal 2.55 mW power consumption. Hardware signal conditioning was provided in the form of programmable gain amplification set to 128V/V, a 5-th order Butterworth design analog low-pass filter with a 100 Hz pass-band (-3dB), and automatic gravitational

offset nulling through the use of a low-noise programmable voltage reference. At the 1024 Sps sampling rate employed, the 5-th order analog low-pass filter provides nearly 80dB of alias frequency rejection.

The conditioned sensor output was sampled at each node by a 12-bit analog-to-digital converter (ADC) at a rate of 1024 Sps then subsequently reconditioned in real-time within the embedded software application using digital signal processing (DSP) through a 16-bitx16-bit hardware multiplier. In this deployment, a complementary 56-th order digital low-pass filter was implemented in the DSP routine to enhance alias signal rejection prior to down-sampling the measurement to an effective rate of 256 Sps. The composite filter results in a DC-97.5 Hz measurement bandwidth (-3dB) with a minimum 74 dB rejection of alias frequencies and increases the effective number of bits of the analog-to-digital conversion by one through the oversampling ratio of four. Given the effective low-pass filter developed from the analog and digital signal conditioning described in this section and the 30 $\mu g / \sqrt{Hz}$ noise density of the accelerometer, the root-mean square noise of the accelerometer is approximately 296 μg over the 97.5 Hz measurement bandwidth. The sensitivity of the accelerometer, signal amplification, and resolution of the converter correspond to an ADC conversion resolution of approximately 8 μg/bit.

2.2.2 Sensor placement

The ambient vibration testing encompassed two instrumentation configurations targeted at balancing the sensor count available with modal reconstruction density and spatial aliasing considerations. The first sensor layout (Fig. 2(a)) consisted of the placement of thirty vertical accelerometers over the

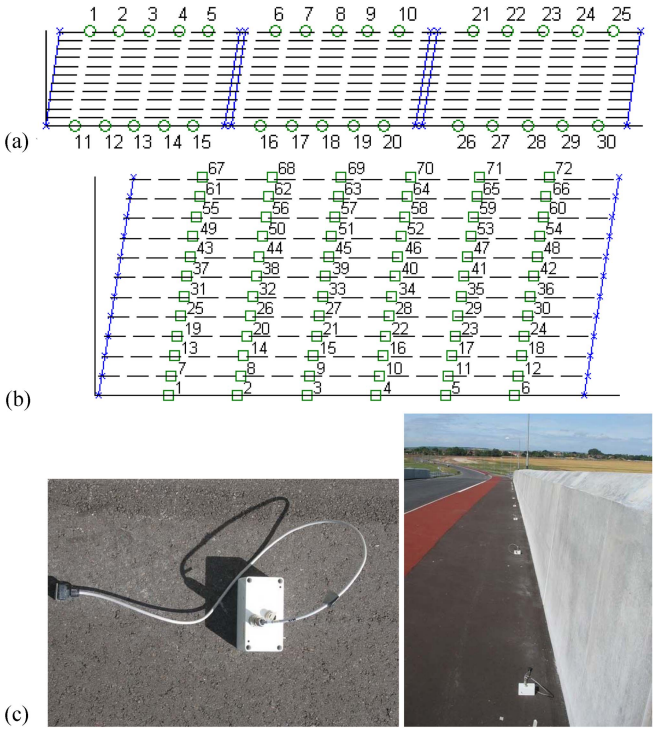

Fig. 2 Instrumentation configurations: (a) stationary vibration sensors for full-span monitoring over exterior beams, (b) reference-based dense vibration monitoring across easternmost span over all beams and (c) accelerometer and wireless sensor nodes installed on deck surfacing

entire span on the deck surfacing alongside the parapets and directly over the exterior beams. Uniform spacing was employed across each span with five sensors allocated per side of the individual spans. Malfunction of the wireless sensor node at location six due to an unknown electrical short caused by a mechanical standoff necessitated removal of this location from the measurement grid; otherwise, there was no issue with any other component of the system hardware. Two construction vehicles were available at the time to provide traffic excitation through repeated, though uncoordinated, passes over the bridge span. Sampling durations of three minutes were specified to capture a large count of vehicle passes and permit high-resolution of the spectral content in the frequency domain. Typical peak acceleration recorded across the sensor array was on the order of 10 mg with most locations witnessing peak accelerations around 6-8 mg.

The first instrumentation configuration provides for the most longitudinally spatially-dense modal reconstruction across the full span, but limits modal reconstruction to the pure bending and first-order torsional mode shapes. To extend the study to higher-order torsional modes, a series of three reference-based ambient vibration tests were performed using a high density layout on the easternmost span (Fig. 2(b)). Sensor location nine in this layout was designated as a fixed reference sensor, while the remaining 29 roving vibration sensors were used to measure the dynamic response at the remaining locations. To cover all 72 locations required recording a total of three reference-based time histories over the network. Due to the use of a highly mobile, wireless platform, the reference-based testing was completed in less than 40 minutes so any temperature variation or time-dependant variation can be assumed to be negligible. During this test program, only a single, smaller truck was available to provide traffic excitation, which resulted in significantly less excitation of the structure as evidenced by the peak accelerations which rarely exceeded 4 mg across the measurement grid.

Given the nature of the loading, the system input was not measurable and the weight of the truck was not determined in the study. Traffic speed was variable and can only be coarsely estimated as typical for local traffic (25 km/hr). Truck passes were not scheduled and their time history is not particularly consequential to the analysis, as with immeasurable system inputs only output-only system identification could be applied. The use of a fixed reference sensor permits the normalization and phase correlation of the three separate test configurations without any knowledge of the truck excitation or periodicity.

3. Operational modal analysis

Given the sufficient levels of excitation during the first configuration testing, operational modal analysis was performed using the frequency domain decomposition, or peak-picking method (Fig. 3). Eigenfrequencies were selected from the peaks in the average normalized power spectral densities calculated over each span individually. The process of mode shape reconstruction was iterative in that the modes for which significant inter-span interaction is present were extracted following the finite element analysis confirming their presence. Positive identification of such modes prior to confirmation through analytical modeling is particularly difficult within output-only system identification as one usually looks for fundamental bending modes and so interaction patterns can sometimes arise spuriously as a combination of closely spaced modes rather than distinct modes.

The first twelve mode shapes identified for the full span are limited to the primary bending and first-order torsional modes due to the spatial limitations of the sensor array. Additional eigenfrequencies were evident in the spectrum, but resulted in spatially aliased mode shapes that could not be used

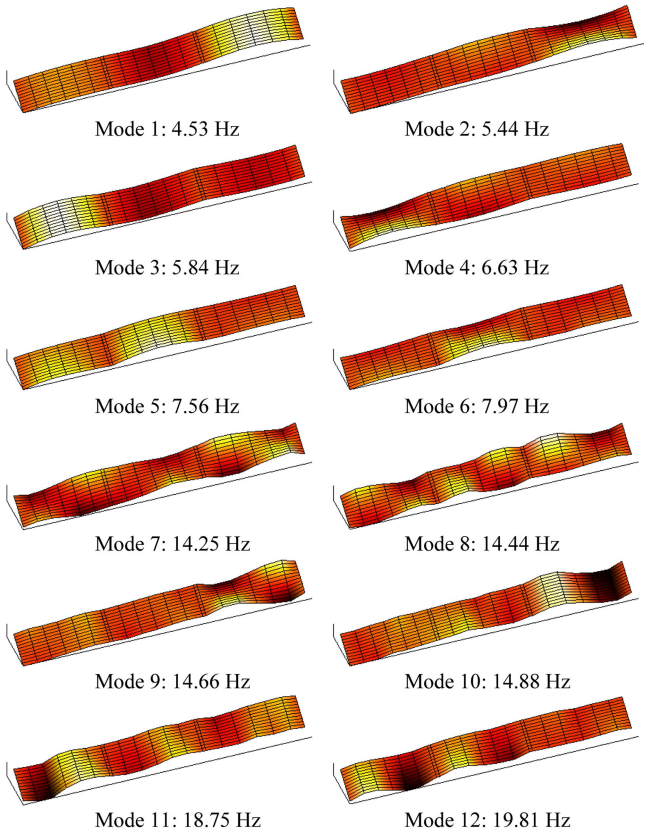

Fig. 3 Mode shapes reconstructed from first instrumentation configuration (Fig. 2(a)) with associated experimental eigenfrequency estimates. Note: Mode shape patterns limited to pure bending and first-order torsional modes due to transverse density of sensor array. Abutment and pier supports assumed to be zero displacement

with confidence in the FE model updating process. To verify the validity of the identified modes in the presence of this aliasing concern and to extend the experimental series of mode shapes for improved model updating, the second sensor configuration (Fig. 2(b)) was utilized to investigate the easternmost span with dense spatial reconstruction.

Data-driven stochastic subspace identification (SSI) was leveraged as a robust output-only system identification methodology for analyzing vibration measurements with low signal-to-noise ratio due to the presence of white process and measurement noise (Peeters 2000). Since a reference-based approach was utilized with three instrumentation configurations sharing a common reference sensor, the analysis had to mesh the results from the individual tests to coordinate the development of span-wide mode shapes without the ease of frequency-based pole selection and enforcement. In this study, the system matrices were estimated for each data set individually and the mode shapes and eigenfrequency estimates were calculated for several model orders to develop a database of possible structural poles as witnessed by each configuration. Given the bandwidth of interest as identified in the prior operational modal analysis, the time series data was first low-pass filtered and decimated to an effective rate of 64 Sps to ease the computational burden and reduce model order to the desired bandwidth. Modal vectors were scaled and oriented for each data set with reference to the

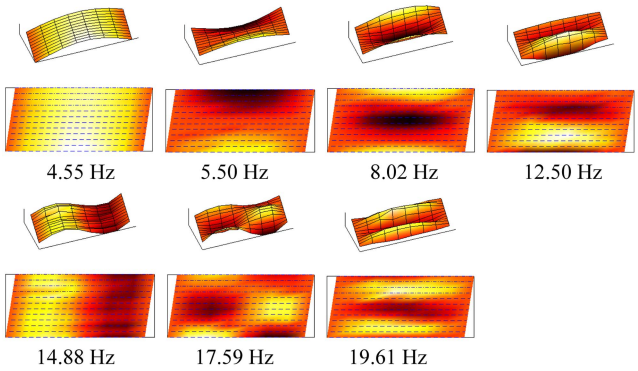

Fig. 4 Mode shapes along with associated experimental eigenfrequency estimates reconstructed for easternmost span from second instrumentation configuration (Fig. 2(b)). Note: Stochastic Subspace Identification used for OMA

stationary sensor to maintain continuity. Since the eigenfrequencies would rarely match exactly across the three state-space models, the mode shapes were then constructed using nearest neighbor eigenfrequencies within reasonable variance (0.05 Hz). This approach was able to reconstruct the first-order bending and torsional patterns up to the fourth order torsional mode as well as the second-order bending mode and its second-order torsional compliment (Fig. 4).

4. Structural identification

A quasi-three-dimensional finite element (FE) model was developed within the ALGOR software framework to model the Nine Wells Rail Bridge using the construction drawings to obtain element geometries and derive cross-sectional properties. The deck was modeled using Veubeke isotropic

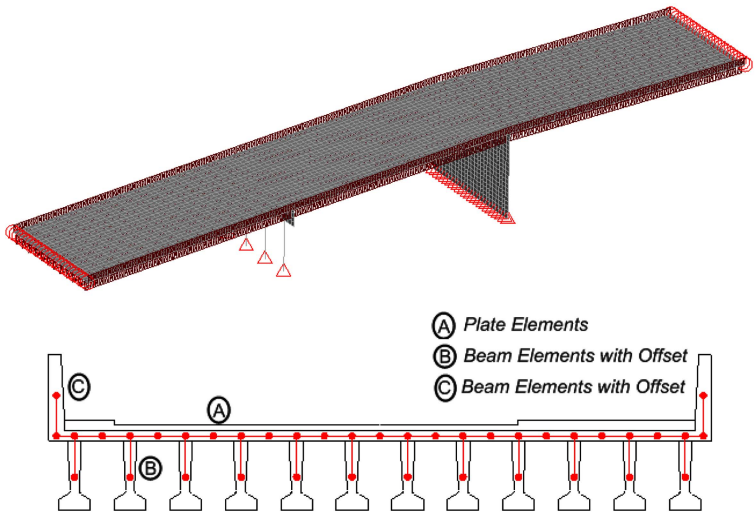

Fig. 5 Finite element model of Nine Wells Rail Bridge and cross-sectional reduction of deck, beams and parapets to plate and beam elements. Note: Preliminary FE model neglects stiffness contribution of deck surfacing, which is represented as a lumped mass proportional to the depth

four node plate elements with sixteen degrees of freedom (MacNeal 1994). The mesh adopted had nodes along the exterior edges of the spans as well as directly over the beams to enforce continuity in the model. Each span consists of a mesh consisting of 42 elements in the longitudinal direction by 24 elements in the transverse direction, for a total of 1008 plate elements per span (Fig. 5). The division of the deck plates into 42 elements in the longitudinal direction was chosen so as to create nodes that coincide with both of the instrumentation layouts from the experimental testing. The built-in materials library was used to specify the deck as medium strength concrete with a mass density of 2405 kg/m^3, 20.7 GPa modulus of elasticity, and Poisson's ratio of 0.15. A plate thickness of 250 mm was assigned, which corresponds to the minimum design depth of the reinforced concrete slab.

The superstructure beams were modeled using 2D beam elements with cross-sectional properties calculated from the precast concrete beam detail drawings. The following cross-sectional properties were employed for each beam element: 0.603 m^2 area, 0.0331 m^4 torsional resistance, 0.165 m^4 moment of inertia about transverse axis through the neutral axis, 0.0131 m^4 moment of inertia about the vertical axis through the neutral axis, and a cross-sectional neutral axis location of 680.5 mm above the bottom edge and centrally located along the transverse direction of the cross-section used for section modulus calculations. The beams were divided into 42 elements along each span consistent with the deck mesh and the material properties were assigned as medium strength concrete. A beam offset was enforced to geometrically locate the cross-sectional neutral axis of the beams below the mid-plane of the deck plate elements consistent with the structural design.

Concerning the prestressing effects on the structural dynamics, there is recent research indicating that prestressing has little or no effect on the natural frequencies of prestressed elements (Hamed and Frostig 2006), and other researchers have adequately performed structural identification of prestressed concrete bridges while neglecting the prestress force (Morassi and Tonon 2008). Consequently, the prestress force has not been accounted for in the FE model adopted for the Nine Wells Rail Bridge. However, it should be noted that the prestressing ensures a fully non-cracked beam section so the effective cross-section can safely be assumed as the entire cross-section.

The precast reinforced concrete parapets were modeled as offset beam elements positioned over the exterior nodes of the deck. Given the sloped cross-sectional shape of the parapets, it was assumed that the average width is 300 mm to produce the following properties: 0.465 m^2 area, 0.0966 m^4 torsional resistance, 0.0931 m^4 moment of inertia about the transverse axis through the neutral axis, and 0.00349 m^4 moment of inertia about the vertical axis through the neutral axis. Consistent with the deck plates, the parapets were divided into 42 elements along each span. The deck surfacing and foot/cycle ways add additional distributed mass across the deck surface without providing significant stiffness contribution. Over the main carriageway, the 125 mm depth of surfacing was converted to an average lumped mass of 100 kg per surface area carried by the nodes. For the foot/cycle way and the curb on the south edge of the spans, this lumped mass was increased to 150 kg per node as a means of accounting for the additional mass associated with the increased depth over the verge. The mass moment of inertia for the foot/cycle way and curb is neglected since it is nominal due to the thin cross-section and respective moment arm associated with the surfacing.

The solid pier between the central and eastern spans was modeled using the same class of plate elements as the deck with the thickness increased to 2 m to reflect the pier thickness. The column supported pier between the western and central spans was modeled using beam elements to represent the columns and plate elements for the portion supporting the beams. The abutments were assumed to be sufficiently inflexible so as to be able to neglect modeling them in favor of enforcing boundary conditions at the beam connections. For the baseline FE model, fixed translational and

rotational displacement boundary conditions were enforced at the lower nodes of the columns and eastern pier. At the beam-to-abutment connections, a pinned connection was provided with the translational displacement fixed, but the rotational displacement unconstrained as a means of accounting for the allowance afforded by the laminated rubber bearings, closed cell foam, and expansion fill. While these boundary conditions are idealizations of the actual conditions, they serve as a reasonably logical starting point for the FE model from which model updating can be used to optimize the restraints to better reflect the measured in-service response.

4.1 Preliminary model comparison

Natural Frequency (Modal) with Load Stiffening analysis was carried out using the ALGOR v23.1 finite element analysis software package. The mode shapes corresponding to the well recognized longitudinal bending and mixed torsional bending modes are presented through the second order bending modes of each span (Fig. 6). Table 1 presents a comparison between the estimated natural frequencies of the low-order mode shapes as determined analytically through the FE preliminary model and experimentally through operational modal analysis. The eigenfrequency index of correlation, Δ, is taken simply to be the percentage difference between the predicted and measured values by

$$\Delta_i = \frac{\lambda_{OMAi} - \lambda_{FEi}}{\lambda_{FEi}} \cdot 100\% \tag{1}$$

where λ_{OMAi} and λ_{FEi} are the eigenfrequencies estimated through operational modal analysis and finite element analysis, respectively.

Eigenvalue estimates are considered in this case to be the appropriate criterion for model updating due to the very low signal-to-noise ratios that preclude high levels of confidence in the absolute accuracy of the modal vectors. However, as a useful measure of the performance of the prediction

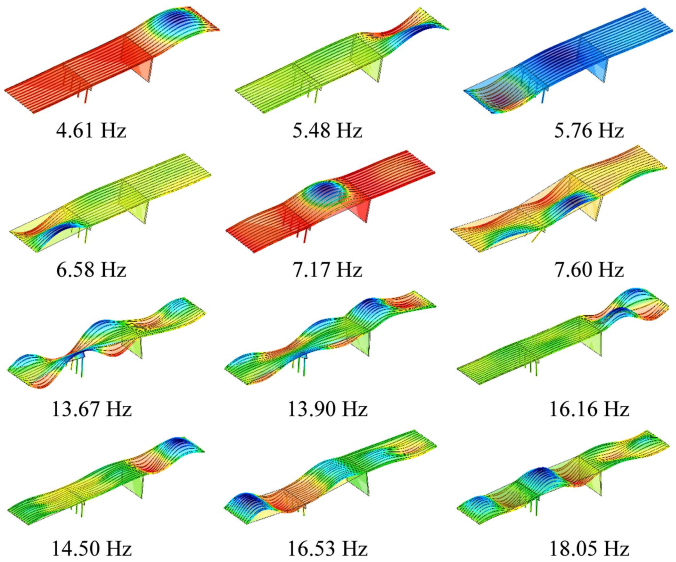

Fig. 6 FEA mode shapes and eigenfrequencies developed from preliminary model corresponding to modes identified in full-span OMA

Table 1 Comparison between baseline analytical (FEA) and experimental (OMA) mode shapes

OMA mode order	OMA freq (Hz)	FEA mode order	FEA freq (Hz)	Δ (%)	MAC
1	4.53	1	4.61	1.8	0.821 / 0.944*
2	5.44	2	5.48	0.7	0.934 / 0.868*
3	5.84	3	5.76	-1.4	0.751
4	6.63	5	6.58	-0.8	0.860
5	7.56	6	7.17	-5.2	0.857
6	7.97	7	7.60	-4.6	0.732
7	14.25	17	13.67	-4.1	--
8	14.44	18	13.90	-3.7	--
9	14.66	22	16.16	10.2	--
10	14.88	20	14.50	-2.6	0.821*
11	18.75	23	16.53	-11.8	--
12	19.81	26	18.05	-8.9	--

Note: MAC values calculated from full-span instrumentation configuration, except for * values, which are calculated from the dense eastern span layout

model, the modal assurance criterion (MAC) was applied to gauge the correlation between the measured and estimated modal vectors from the analytical model. The MAC is a scalar indicator with a long history in vibration-based structural identification and damage detection (Allemang 2003). The MAC value of interest to this study is applied to the measured and predicted modes of the same order and can be calculated for each mode shape through

$$MAC_i = \frac{(\phi_{OM\,Ai}^T \phi_{FEi})^2}{(\phi_{FEi}^T \phi_{FEi})(\phi_{OM\,Ai}^T \phi_{OM\,Ai})} \tag{2}$$

where $\phi_{OMA,i}$ and $\phi_{FE,i}$ are the modal vectors for the i-th mode as determined through the operational modal analysis and finite element analysis, respectively. The modal vector for the FEA results was reduced to the nodes coinciding with sensor locations. The index was limited to modes with sufficient spatial measurement density for absolute confidence in identification and was performed separately for the full-span and reference-based test configurations.

In this case study, the finite element model displays surprisingly good correlation with the measured response as the natural frequencies are generally within a few percent of the measured values and the mode shapes themselves visually compare quite favorably. Quantitative correlation through the MAC value index reveals relatively favorable correlation for most modes, though the values are lower than typically desired for a final analytical model. However, the general consistency with the experimental data might warrant consideration of the preliminary model as sufficient for use as an analytical and evaluation tool. In this study, it is taken as an ideal starting point for model updating using additional measures of correlation, specifically an extension to higher-order mode shapes as permitted through the supplemental reference-based deployment.

Utilizing the reference-based dense deployment of accelerometers on the easternmost span provides an extended subset of mode shapes for comparison with the FE model prediction (Fig. 7). From these modes, it is apparent that the FE model underestimates the torsional restraint in the

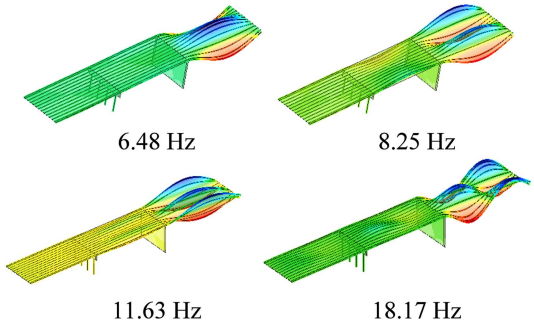

Fig. 7 Extended set of FEA mode shapes and eigenfrequencies developed from preliminary model corresponding to higher-order torsional modes on the easternmost span identified in reference-based OMA

Table 2 FEA comparison of higher-order torsional modes reconstructed through OMA of reference-based testing on easternmost span of structure

Eastern span mode	FEA freq (Hz)	OMA freq (Hz)	Δ (%)	MAC
First-order bending pattern				
2nd Torsion	6.48	8.02	-19.2	0.885
3rd Torsion	8.25	12.50	-34	0.774
4th Torsion	11.63	19.61	-40.7	0.705
Second-order bending pattern				
2nd Torsion	18.17	17.59	3.3	0.742

Note: MAC values calculated from the reference-based testing limited to the easternmost span

bridge spans thereby producing artificially low estimates of the eigenfrequencies for the higher-order torsional modes (Table 2). The value of the supplemental spatially dense deployment is therefore extolled through the fact that this strong discrepancy would otherwise be hidden in the structural identification and the preliminary model would be assumed to be well correlated. The identification of this strong inconsistency between the predicted and measured response was only afforded through the reference-based deployment as enabled through the highly mobile and expedient to use wireless sensor network. Since the preliminary FE model already reconstructs the first-order bending and torsion modes for each span with strong correlation to the experimental results, the subsequent model updating will need to stiffen the response over the higher-order torsional modes without significantly affecting the eigenfrequencies of the already well-tuned modes.

4.2 Model updating

Model updating is the iterative process whereby the parameters associated with the boundary conditions and material properties are adjusted to best fit the numerical model to the experimental response measurements. There is no definitive process for undertaking this model tuning, particularly for ambient vibration data, and there is a great degree of subjectivity and reliance on engineering judgment and experience to select the appropriate parameters to adjust to improve the correlation between the model and the measured response. Most structural identification techniques employ some iterative process to optimize the difference between analytical and experimental estimates of the modal parameters and/or indices derived from the modal parameters (Jaishi and Ren 2005,

Morassi and Tonon 2008). As a general disclaimer, it should be noted that the solution to this optimization problem is non-unique and therefore does not guarantee that the end parameters and properties translate with certainty to the real-world conditions.

Sensitivity analysis was conducted to determine the effect of the boundary conditions as well as the elastic modulus of the reinforced concrete deck on increasing the eigenfrequency separation between the lower-order and higher-order torsional modes to better reconstruct the measured response. However, these approaches were found to be unsatisfactory in that in each case they generally produced uniform or insufficiently small frequency shifts rather than producing the increase in eigenfrequency required for the higher-order torsional modes. To obtain the desired separation, it was found that the deck thickness had to be increased to produce the necessary increase in stiffness to resist the torsional response.

The deck thickness in the roadway was increased to 375 mm, which corresponds to the required 250 mm design thickness of the reinforced concrete deck and the 125 mm minimum surfacing layer. For the plate elements where the curb and footway exist, a total deck thickness of 500 mm was specified to account for the additional surfacing consistent with the curb height. The nodes of the deck plates were proportionally displaced as well to correctly position the mid-plane of the deck for proper geometry and correct beam offsets. It should be noted that, in this case of model updating, the authors are not modifying the geometric design of the span, but rather accounting for the stiffness contribution of the asphalt surfacing layer in the model rather than simplifying it to the associated dead-load.

The revision in modeling the surfacing as integral to the deck produced the necessary increase in the eigenfrequencies of the torsional modes in the easternmost span to reconstruct the measured response within eleven percent. In the updated model, the boundary conditions at the abutments remain pinned, though rotational restraint was also fixed about the longitudinal and vertical axes and rotational springs were added to restrain motion about the transverse axis. Eigenvalue sensitivity analysis produced optimal spring constants of 2e7 N·m/rad at the eastern abutment and 1.5e9 N·m/rad at the westernmost abutment. The optimization routine focused on minimizing the percent difference in eigenfrequency estimate for the primary and first-order torsional modes of the outer spans, which are most affected by these rotational springs. It should be noted that the design details are consistent for the two abutments and would suggest consistent rotational spring constants. The authors can only speculate that the geometric differences associated with the deck slope, skew, and span length contribute to the discrepancy in applied spring constant required to enforce continuity between the experimental and analytical results.

For nearly all of the mode shapes included in the updating process, the revised model produced better correlation with the measured eigenfrequencies and for those in which the correlation is worse, the degree of change is nominal (Table 3). Correlation between the modal vectors, as indexed by the MAC values, was also found to improve for most mode shapes. In particular, the primary and first-order torsional modes of the outer spans witnessed substantial improvement in MAC correlation through the model updating. When the predicted mode shapes are compared to those measured (Fig. 8), it becomes evident that the improvement in modal vector correlation arises largely from improved estimation of the coupled response across the spans in the optimized model. The experimental measurements clearly identify coupled motion between the spans, i.e., the central span experiences measurable deflection within the primary mode of the easternmost span. In contrast, the preliminary FEA results were sharply characterized by a general isolation of the displacement response within the spans experiencing typical modal patterns. This phenomenon further supports the decision to

Table 3 Comparison between optimized FEA model and measured response through eigenvalue indices and MAC

Mode shape	OMA freq (Hz)	FEA 2 Freq (Hz)	Δ (%)	MAC config #1	MAC config #2
East P	4.53	4.53	0	0.962	0.974
East T1	5.44	5.44	0	0.992	0.894
West P	5.84	5.72	-1.9	0.885	--
West T1	6.63	6.75	1.8	0.922	--
Center P	7.56	7.51	-0.7	0.802	--
Center T1	7.97	8.28	-3.9	0.812	--
East T2	8.02	7.17	-10.6	--	0.927
East T3	12.50	11.38	-9.0	--	0.762
East 2T	14.88	14.51	-2.5	--	0.835
East 2T2	17.95	18.62	5.9	--	0.804
East T4	19.61	19.36	-1.3	--	0.579

Note: P–Primary longitudinal bending mode; aTb–bth torsional bending pattern of ath longitudinal bending order

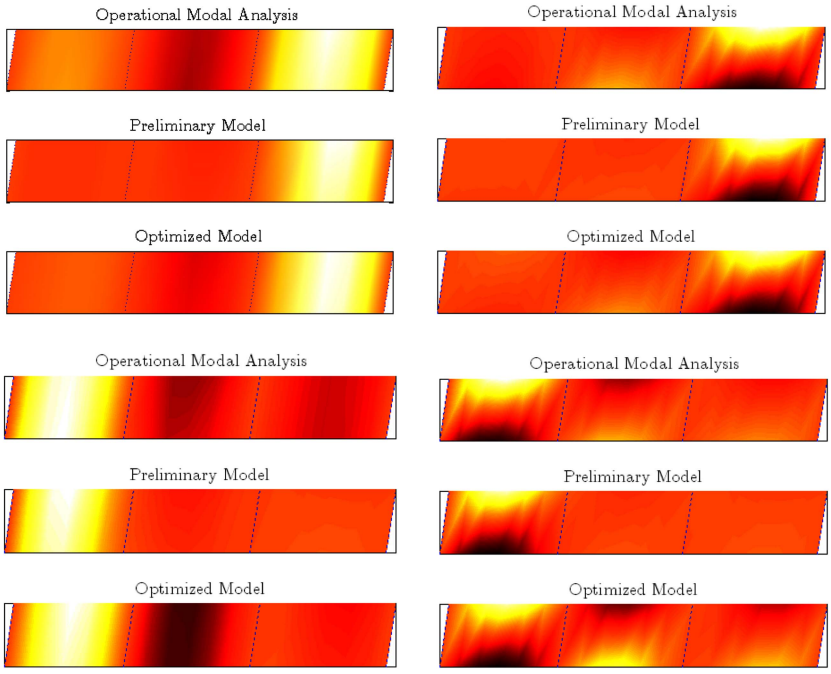

Fig. 8 Comparison of the lower-order mode shapes as measured in the experimental study, predicted in preliminary FE model, and estimated in optimized FE model. Note: FE modal vectors reduced to nodes coinciding with sensor locations to maintain consistency with experimental modes

increase the deck thickness in the model as such a span-isolated response in the preliminary FEA model would suggest that the relative stiffness of the deck to the piers was disproportionately low. Following model updating with the revised modeling of the deck surfacing and optimized boundary conditions, the prediction model more accurately predicts the coupled response across the spans.

While at this stage the model appears to be a reliable reconstruction of the as-built construction, one of the caveats in iterative model updating is that the optimization is inherently biased toward the modes selected for inclusion in the updating process. In this study, the primary and first-order torsional modes of each span were selected due to spatial aliasing concerns in the full-span deployment and the modal parameter set was supplemented with higher-order torsional modes specific to the eastern-span as permitted through the dense reference-based testing. In total, ten mode shapes are included in the model updating, which compares favorably with similar structural identification studies (Morassi and Tonon 2008, Jaishi and Ren 2005) and is generally considered a substantial set. This particular set encompasses a significant portion of the lowest frequency modes exhibited by the structure. The higher-order modes excluded due to spatial resolution restrictions imposed by the measurement grid are generally associated with larger eigenfrequencies than those included in the updating process. Since the modal flexibility matrix is inversely proportional to the natural frequencies of the mode shape contributions (Toksoy and Aktan 1994), it follows that the excluded higher-order modes will have significantly less effect on the overall structural response and therefore correlation is less critical for these modes. This has been further evidenced by the work of Catbas *et al*. (2006), in which the modal flexibility matrix and analytical deflection of girders as computed from the modal flexibility matrix was found to converge after inclusion of a finite number of modes. The authors in that study found that ten modes were sufficient for convergence using measurements from a three-span reinforced concrete deck on steel stringer bridge. Since at least an equal number of modes were found to correlate well with the experimental results in the present study, the analytical model obtained through system identification is deemed sufficiently optimal and can reasonably be extended to static analyses, such as to estimate the deflection arising from prescribed loading scenarios.

5. Conclusions

High-rate, real-time wireless sensor networks facilitate rapid instrumentation of highway bridges for large-scale, dense operational modal analysis to estimate the in-service modal parameters. Such experimental estimates are particularly beneficial for validation and dynamic tuning of simplified analytical models through structural identification to derive a reliable and accurate representation of the structure with consideration of the as-built conditions. The end result is an analytical tool potentially suited for updating structural response predictions.

This study utilized a thirty channel wireless sensor network with low-cost MEMS accelerometers to expediently obtain traffic vibration response measurements over a 128 Hz signal bandwidth (256 Sps sampling rate). Testing was performed with multiple instrumentation layouts for a spatially clear representation of sixteen mode shapes, of which ten were utilized in structural identification. A quasi-three-dimensional finite element model of the bridge was constructed using plate and beam elements and then model updating was performed to calibrate the model to the measured response. Strong correlation of the general pattern characteristics and mode shape orders was evident between the experimental and analytical models with exceptional correlation in natural frequency estimates as obtained through optimization of a selection of ten fundamental modes. A primary strength of rapidly deployable and highly mobile wireless accelerometers within ambient vibration monitoring is the ease and expedience within which dense reference-based operational modal analysis can be performed. As evidenced in this study, this permits for improved structural identification by permitting an extended set of mode shapes for correlation during model updating.

From the structural identification carried out in this study, there are two primary conclusions that may be drawn from the model updating process regarding what is deemed to be the most appropriate representation of the structural elements. Foremost, the deck surfacing, curbs and cycle-ways should be modeled as structural elements with stiffness as well as mass contribution. In some studies, asphalt wear surfaces are neglected or accounted for solely as dead load. This may be an advisably conservative approach for design purposes but was found to produce artificially low estimates of the eigenfrequencies associated with higher-order torsional mode shapes. Second, the strong correlation between the developed model and the experimentally measured bridge response indicates that structural identification can be successfully accomplished for prestressed reinforced concrete designs without accounting for the prestress force. This may either suggest that the effect can be lumped into the translational boundary condition or serve as evidence in support of Hamed and Frostig (2006) who concluded negligible effect of prestress force on modal parameters.

Acknowledgments

The authors gratefully acknowledge the assistance provided by Tom Williams and John St. Leger of Atkins Global, John Clough and Cambridgeshire County Council, and Colin Himpett of Jackson Civil Engineering. Furthermore, the authors wish to recognize the on-site assistant with sensor installation and field logistics provided by Dr. Peter Bennett, Peter Knott and Martin Touhey of the University of Cambridge.

References

Aktan, A.E., Catbas, N., Türer, A. and Zhang, A. (1998), "Structural identification: analytical aspects", *J. Struct. Eng.-ASCE*, **124**(7), 817-829.

Allemang, R.J. (2003), "The modal assurance criterion (MAC): twenty years of use and abuse", *Sound Vib. Mag.*, **37**(8), 14-21.

Catbas, F.N., Brown, D.L and Aktan, A.E. (2006), "Use of modal flexibility for damage detection and condition assessment: case studies and demonstrations on large structures", *J. Struct. Eng.-ASCE*, **132**(11), 1699-1712.

Hamed, E. and Frostig, Y. (2006), "Natural frequencies of bonded and unbonded prestressed beams-prestress force effects", *J. Sound Vib.*, **295**(1-2), 28-39.

Jaishi, B. and Ren, W.X. (2005), "Structural finite element updating using ambient vibration test results", *J. Struct. Eng.-ASCE*, **131**(4), 617-628.

MacNeal, R.H. (1994), *Finite Elements: their design and performance*, Marcel Dekker, USA.

Morassi, A. and Tonon, S. (2008), "Dynamic testing for structural identification of a bridge", *J. Bridge Eng.*, **13**(6), 573-585.

Peeters, B. (2000), *System Identification and Damage Detection in Civil Engineering*, PhD Dissertation, Katholieke Universiteit Leuven.

Toksoy, T. and Aktan, A.E. (1994), "Bridge condition assessment by modal flexibility", *Exp. Mech.*, **34**(3), 271-278.

Whelan, M.J. and Janoyan, K.D. (2009), "Design of a robust, high-rate wireless sensor network for static and dynamic structural monitoring", *J. Intel. Mat. Syst. Str.*, **20**(7), 849-863.

Whelan, M.J., Gangone, M.V., Janoyan, K.D. and Jha, R. (2009a), "In-service modal analysis of a highway bridge using a real-time wireless sensor network", *Eng. Struct.*, **31**(10), 2224-2235.

Whelan, M.J., Gangone, M.V. and Janoyan, K.D. (2009b), "Highway bridge assessment using an adaptive real-time wireless sensor network", *IEEE Sens. J.,* **9**(11), 1405-1413.